MICROBIALLY MEDIATED DEPOSITION OF POSTGLACIAL TRANSITION LAYERS FROM THE NEOPROTEROZOIC OTAVI GROUP, NAMIBIA: EVIDENCE OF RAPID DEGLACIATION AFTER THE STURTIAN CRYOGENIC PERIOD

Ildikó GYOLLAI[1,2], Márta POLGÁRI[3*], Krisztián FINTOR[4], Friedrich POPP[5], Dieter MADER[1], Elemér PÁL-MOLNÁR[4,6], Szabolcs NAGY[2,4] & Christian KOEBERL[1,7]

[1]*Department of Lithospheric Research, University of Vienna, Althanstrasse 14, A-1090 Vienna, Austria*
[2]*Cosmic Materials Research Group, Geobiomineralization and Astrobiological Research Group, Eötvös Loránd University of Budapest, 1117 Budapest, Pázmány P. Street 1/A, Hungary*
[3]*Research Center for Astronomy and Geosciences, Geobiomineralization and Astrobiological Research Group, Institute for Geology and Geochemistry, Hungarian Academy of Sciences, 1112 Budapest, Budaörsi Street 45, Hungary, e-mail: rodokrozit@gmail.com, *corresponding author*
[4]* Department of Mineralogy, Geochemistry and Petrology, University of Szeged, 6722 Szeged, Egyetem Str. 2, Hungary*
[5]*Department of Geodynamics and Sedimentology, University of Vienna, Althanstrasse 14, A-1090 Vienna, Austria*
[6]*MTA-ELTE Volcanology Research Group, H-1117 Budapest, Pázmány P. Street 1/C, Hungary*
[7]*Natural History Museum, Burgring 7, A-1010 Vienna, Austria*

Abstract: Iron-rich postglacial transition layers from early Cryogenian "Snowball Earth" sedimentary environments of the Otavi Group (Namibia) were studied by microtextural high-resolution mineralogical and geochemical methods. Series of Fe-rich biomats (goethite, hematite) were identified, and signs of diverse microbial, filamentous Fe-oxidizing, and cyanobacterial activity were documented for the first time. The matrix mineralogy consists of quartz and dolomite, diverse organic matter, muscovite, apatite, and pyrite. On the basis of mineralized bacterial layering of the Fe-rich biomats, the postglacial transition layers are interpreted to have formed within a few hundred years under suboxic, neutrophilic, shallow, fresh- to brackish-water conditions during an initial rapid deglaciation process from a Neoproterozoic "Snowball Earth" environment. Thus we suggest that the overlying Rasthof cap carbonates, influenced by tectonic subsidence of the region, may also have been deposited within a very short period, comprising the entire deglaciation process.

Keywords: Sturtian, Snowball Earth, microbial mats, deglaciation, transition layer, iron-oxidizing bacteria

1. INTRODUCTION

Neoproterozoic glaciations of global extent occurred within three succeeding cryogenic periods: (i) the Sturtian period (720–660 Ma, type location: Sturt valley, South Australia), (ii) the Marinoan period (650–635 Ma, type location: Marino, South Australia) (Arnaud et al., 2011; and references therein) and (iii) the Gaskiers period (ca. 580 Ma, type location: Gaskiers, Newfoundland, Canada), each glaciation lasting several million years (e.g., Kennedy et al., 1998; Bodiselitsch et al., 2005). The term "Snowball Earth" was introduced in the year 1992 (Kirschvink, 1992; Hoffman et al., 1998). A variety of hypotheses have been formulated to

explain various aspects of the Cryogenian global(?) glaciations (Fairchild & Kennedy, 2007), with the most important being: (i) Hard Snowball Earth (Hoffman et al., 1998; Hoffman & Schrag, 2002), (ii) Slushball Earth (Harland & Rudwick, 1964), (iii) Zipper-rift model (Eyles & Januszczak, 2004) and (iv) High-tilt Earth (Williams, 1975).

Similarities to Paleoproterozoic diamictites are noticeable, e.g., some of the Cryogenian (Sturtian) diamictites are also saturated with iron precipitations. Banded iron (±manganese) formations (BIFs) occur within glacial marine formations in Namibia (Martin, 1964), Australia (Whitten, 1970), Canada (Klein & Beukes, 1993), and Brazil (Klein & Ladeira, 2004; Hoffman et al., 2011).

Large Neoproterozoic Fe and Fe-Mn deposits developed within a paleolatitude range around 35° (Hoffman & Li, 2009) holding a thickness variation from tens to hundreds of meters. These deposits indicate that the ancient glacial deep waters became anoxic, allowing Fe^{2+} and Mn^{2+} ions supplied by mid-ocean ridge hydrothermal systems to travel widely in solution (Martin, 1964). That dissolved Fe(II) must be oxidized to Fe(III) in order to precipitate as a precursor substance of the BIFs, which could occur wherever oxic waters were supplied (e.g., subglacial meltwater discharges at marine ice grounding lines) or could even be generated by phototrophic bacteria in places of marine environments where ice was cracked or thin (Konhauser et al., 2002; Kappler et al., 2005). These BIF layers were overlain by cap dolostone. The contact between Sturtian glaciogenic deposits, and its cap-carbonates is characteristically singular, smooth, abrupt and conformable (Hoffman et al., 2011), and that is also the case for the parallel-laminated, Fe-rich formations that mark the contact zone at the studied localities.

The paleogeographic rearrangement due to the break-up of Rodinia allowed newly-arranged sea currents to provide an effective source of nutrients, such as Fe and P, to equatorial sea water. As a result, the already existing biodiversity (algae and cyanobacteria) increased and consequently increased the production rate of photosynthetic oxygen (Campbell & Squire, 2010). This process changed the redox state of the ancient oceans and atmosphere (Knoll, 2003). Scientists advocate the existence of ice-tolerant biomats during the period of Cryogenian glaciations and compare that with present-day polar ice biota in regions of Antarctica (dominated by, e.g., filamentous cyanobacteria and diatoms; Vincent & Howard-Williams, 2000). The modern-day sea ice biota is dominated by diatoms, and the polar ice shelf communities are dominated by oscillatorian cyanobacteria, a group that is widely distributed in the Archean and Proterozoic fossil records (Vincent et al., 2000; Schopf, 2004).

The oldest known microbial mats were discovered in the early Archean (3.2 Ga) Moodies Group, where the organic residue of biomats have biogenic isotopic signatures ($\delta^{13}C \sim -20$ ‰) closely associated with hematite, goethite and chert (Noffke et al., 2006). Similar structures from the upper Neoproterozoic Nama Group, Namibia, have been described (Noffke et al., 2002). These fossilized biomats, which occur in a higher stratigraphic position (younger occurrence) than our findings, have carpet-like structures and are composed of bacterial cells together with their mucous extracellular polymeric substance (EPS) (Noffke et al., 2003).

We consider the postglacial transition layers (Chuos Fm / Rasthof Fm) of the Namibian Otavi Group as an example of a series of ancient Fe-rich biomats formed at the sediment/water interface. Moreover we emphasize the importance of this mineralized, microbially produced, sedimentary structure system (MMPSS), studied first as microbialite, which offers a novel chance for the estimation of paleoenvironmental conditions and the duration of related sedimentary cycles. Besides we advocate a comparison with rapid, present-day climate change models. Here, we present results and interpretations of our geochemical, microtextural and micromineralogical analysis.

2. GEOLOGICAL BACKGROUND OF SAMPLE AREAS

The Sturtian postglacial transition layer studied here spans the uppermost/lowermost portion of the Chuos/Rasthof Formation (Fig. 1). Massive to poorly stratified diamictite is the characteristic lithology of the glaciogenic Chuos formation, deposited during the initial rifting phase of Rodinia at a paleolatitude around 35° (Christie-Blick et al., 1999; Eyles & Januszczak, 2004). Deposits of the Chuos Formation are widely exposed throughout the Northern Platform Area, varying both regionally and locally in thickness, being thickest (up to ~1000 m) in paleodepressions and absent on paleo-heights (Martin, 1964). Toward the outer platform edge and foreslope area, the diamictite thins to virtually zero, but accumulates in the foreslope area. The diamictites are interpreted as originating mainly from glacial marine rain-out deposits formed close to the grounding line of warm-base ice streams (Hoffman & Halverson, 2008).

At the upper contact of the Chuos Formation, layers are almost invariably sharp and smooth, being genetically interpreted as an abrupt flooding surface separating the diamictite from the deepwater dolomite rhythmite of the basal Rasthof Formation, which displays no evidence of reworking, subaerial exposure or significant hiatus (Hoffman & Halverson, 2008). However, at our C13 sample locality (Sesfontain-Opuwo Road) the upper part of the Chuos Formation is composed of siliciclastic, Fe-saturated debris and crystalline pebbles derived from Proterozoic basement source. The outcrop´s lower part displays a different composition of carbonate debris - and pebbles eroded from former shelf deposits (Ombombo Subgroup), hence this depositional trend displays enormous erosive wear of glacier ice in Sturtian times.
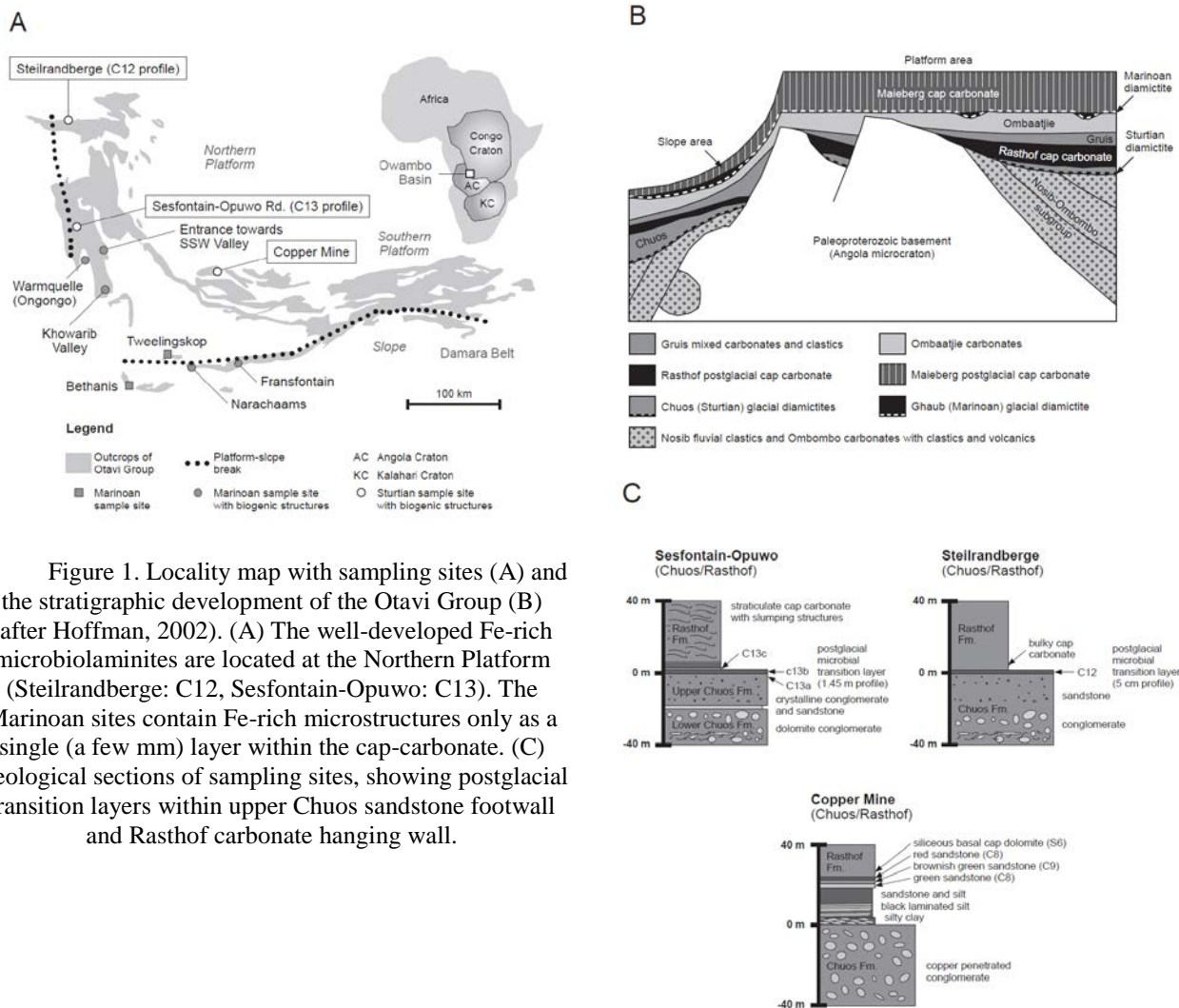
Figure 1. Locality map with sampling sites (A) and the stratigraphic development of the Otavi Group (B) (after Hoffman, 2002). (A) The well-developed Fe-rich microbiolaminites are located at the Northern Platform (Steilrandberge: C12, Sesfontain-Opuwo: C13). The Marinoan sites contain Fe-rich microstructures only as a single (a few mm) layer within the cap-carbonate. (C) Geological sections of sampling sites, showing postglacial transition layers within upper Chuos sandstone footwall and Rasthof carbonate hanging wall.

The Rasthof Formation, normally 200-400 m thick on the Otavi Platform, has a layer-cake internal stratigraphy comprised of three members termed "abiotic", "microbial", and "epiclastic". The basal "abiotic" member of the Lower Rasthof Formation consists of flaggy, dark gray dolomite and dolomitic limestone, characterized by mm-scale, parallel, turbiditic lamination. Hematite, mobilized from the underlying diamictite, stains the basal few centimeters of the dolomite rhythmite (Hoffmann & Halverson, 2008).

The "microbial" member, which is one focus of this work, may rest directly upon Chuos diamictites in tectonically elevated regions (our samples C13), indicating that the mentioned terms "abiotic" and "microbial" do not represent stratigraphic but facies features. Furthermore, even the "epiclastic" member can be recognized in this tectonically elevated region, thus providing a chance for stratigraphic correlation of time-equivalent facies regions.

Our samples location at Sesfontain-Opuwo Road (Table 1, C13 - 5 samples) stands within an area of the Northern Platform that was affected by tectonic folding of the eastern Kaoko Zone (Fig. 1, Table 1). At this locality our samples from the transition zone between Chuos diamictites and Rasthof cap carbonates represent the stage of a shallow, fresh- to brackish-water platform-island environment. Field observations indicate that unstratified Chuos diamictites are topped by their own reworked material revealing stratified textures. This trend was detached by the onset of laminated carbonate deposition (based on new field observations by F.P. [2013] in the proximity of the Sesfontain-Opuwo Road locality our C13 samples profile is de facto the lower part of a 1.45 m thick layer). The reworking stage at the diamictite's top (represented by our samples C13a, b) means that apparently glacial mediated sediment supply ceased (because of vanishing glacier ice) and the sea level increased. Hence the study area was flooded with oversaturated sea water (from upwelling zones) triggering the precipitation of carbonate mud. We consider these specific environmental conditions at the beginning of crustal subsidence/sea level rise

being appropriate with respect to the formation of biomats.

This assumed glacial transition zone, represented with our samples C13 is obviously stained by iron-saturated fluid migration arising from the underlying Chuos diamictites (iron-oxide mineralization).

Our Steilrandberge locality (Table 1, C12 - 1 sample) is situated within the Steilrandberge Syncline of the Northern Platform Area (Fig. 1, Table 1). Because of its proximal position within the evolving Otavi Platform, the diamictites accumulated reportedly in that area to a thick pile (up to 1000 m) in Chuos times (Hoffman & Halverson, 2008). The transition of these diamictites to a cap-dolomitic layer (sample C12) is the focus of interest at this site. On the basis of field observations our sample (C12) is a thick bedded, microcrystalline dolomite, indicating its formation within a higher platform-like environment.

The sample itself spans the top of the diamictite, as well as the lower part of its cap-carbonate, where it shows signs of diverse putative microbial activity (also Fe-rich forms) from which the most representative presumably microbiolaminite layers are chosen for analysis.

Table 1. Location and description of samples from Copper Mine (C8-C10), Steilrandberge (C12) and Sesfontain Opuwo Rd. (C13) localities

Stratigraphical setting	Sample	Location	Lithology	Mineral composition	Microbial structures
Basal Rasthof Formation	C13c	Sesfontain-Opuwo Road (18°46'26.49"S; 13°45'11.24"E)	Fe-rich microbialite Strong weathering of biogen structures	70 wt% dolomite 30 wt% goethite, hematite, quartz	filamentous (tubular) forms unnamed colonial coccoid cells, and spheroidal unicells
	C8	Copper Mine (9°25'18.43"S; 15° 9'50.90"E)	Oolitic sandstone	carbonate: 75 wt% mica: 8 wt% kalifeldspar: 7 wt% quartz: 10 wt% 5 wt% clay, iron-oxide, zircon, barite	calcification bacterial communities around ooids and oncoids
Chuos/Rasthof Formation boundary	C12	Steilrandberge (17°47'1.67"S; 13°39'54.10"E)	silt Fe-rich microbialite	70 wt% goethite, hematite, 30 wt% quartz,	filamentous (tubular) forms sheath-enclosed colonial unicells
	C9	Copper Mine (9°25'18.43"S; 15° 9'50.90"E)	Carbonate-quartzite silt	carbonate: 70 wt% iron-oxide: 15 wt% quartz: 10wt% mica: 5wt%	no
	C13b2 C13b1	Sesfontain-Opuwo Road (18°46'26.49"S; 13°45'11.24"E)	Fe-rich microbialite	60-70 wt% goethite, hematite 5-10 wt% dolomite 15 wt% quartz 10 wt% mica	filamentous (tubular) forms unnamed colonial coccoid cells, diatoms (similar to present Navicula), filamentous cyanobacteria
Chuos Formation (top)	C13a2 C13a1	Sesfontain-Opuwo Road (18°46'26.49"S; 13°45'11.24"E)	Fe-rich microbialite	50-60 wt% goethite, hematite, 20-30 wt% dolomite, 10 wt% quartz, 5-10 wt% mica	filamentous (tubular) forms unnamed colonial coccoid cells, sheath-enclosed colonial unicells
	C10_2 C10_1	Copper Mine (9°25'18.43"S; 15° 9'50.90"E)	Fine sandstone, segregated terrestrial components in mudstone	carbonate: 40-70 wt% quartz: 10-20 wt% iron-oxide: 10% mica (sericite), chlorite: 5-9 wt% clay: 6 wt% feldspar: 5 wt%	unnamed colonial coccoid cells, sheath-enclosed colonial unicells in recrystallized quartz - filamentous (tubular) forms in iron oxide

C13 represents a 1.45 m -, C12 a 50 mm thick profile

Generally, the sampled Fe-rich transition layers (from both the Sesfontain-Opuwo Road and Steilrandberge localities) exhibit continuous and conformable internal parallel laminations hallmarked by sharp basal and upper contacts and variable thickness.

Putative biogenic relicts were also found at our Cooper Mine locality (Table 1, Samples C8, C9, C10). There, intensified debris input (feldspar, quartz, zircon, quartz pebbles, etc.), as well as higher energetic aquatic conditions (oolites), anticipated most likely the development of well stratified, Fe-rich layers., but signs of iron-oxidizing bacteria (FeOB) occur as thin biofilms covering ooides and quartz grains. However, the boundary layer of Copper Mine locality (sample C9) does not contain any microbial structures of iron-oxidizing bacteria, hence this iron-rich layer is derived by input of continental weathering, but at the top of diamictite layers (sample C10) FeOB colonies are visible at rims of iron-bearing minerals (e.g., chlorite) originated due to biodegradation. Our samples from the Marinoan postglacial transition layer (Fig. 1) also exhibit putative microbial structures of iron-oxidizing bacteria (FeOB) and mineral alteration forms, but their preservation state is poor, hence the Marinoan section is not discussed here in detail. As all the studied localities belong to internal platform environments, well-developed biomats may be favored preserved under predominant starving conditions without terrigenous input and a required low energy aquatic system.

3. METHODS

The mineral compositions of the bulk samples were determined by X-ray powder diffraction (XRD) at the University of Vienna. Diffraction data were collected with a Phillips diffractometer (PW 3710, goniometer PW-1820) with CuK_α radiation (45 kV, 35 mA), a step size of 0.02 degrees and a counting time of 1 s per step. Minerals were identified using the Joint Committee on Powder Diffraction Standards database (JCPDS, 1980).

Detailed micro-Raman investigation was made on two selected thin sections (C13b2, C13c). A Thermo Scientific DXR Raman Microscope was used, with a 532 nm (green) diode pumped solid-state (DPSS) laser with a Nd-YAG source crystal. Measurements were made under 1.5 mW laser power using a 50x objective lens in confocal mode (confocal aperture 25 μm slit). The acquisition time was 1 min and the spectral resolution was ~2 cm^{-1} for each measurement (Szeged University, Hungary). The distance between two measured points was 50 μm.

Raman spectra acquired for samples were organized into diagrams (n: 1032). 372 spectra were acquired in sample C13b2 and 660 spectra were acquired in sample C13c.

Petrographic structural-textural studies were undertaken using five oriented (bottom and top of sequence position) thin sections using a NIKON ECLIPSE 600 optical petrographic microscope in Budapest, Hungary.

4. RESULTS

The oriented samples macroscopically resemble series of Fe-rich biomats occurring as millimeter-scale microbiolaminite (Fig. 2A, B). No signs of erosion or any other hiatus were observed in the studied profile. The light and red laminae are variable in thickness and frequency of occurrence; however, they define a more or less regular, millimeter-scale rhythmic lamination in the samples.

The thin sections show a fabric-like lacework texture within the very fine-grained dolomite and quartz matrix, described as an interwoven, filamentous meshwork. The range of thicknesses of the mineralized filamentous structures is approximately 1-10 μm (Fig. 2C). The filaments are capped by a homogeneous mineral covering, generally goethite and rarely hematite, according to the Raman analyses. Solitary carbonate clusters and quartz matrix material float or are embedded within the laminated matrix without grain-to-grain contact. These intervals show diffuse contacts. The biomats are often so dense that they form an opaque mineralized segment (Fig. 2B). The matrix of the goethite and hematite structures consists of dolomite and/or quartz and organic matter as the main components. Filamentous (tubular) forms of unnamed colonial coccoid cells, sheath-enclosed colonial unicells and spheroidal unicells also occur in the sections (Fig. 2C). The presence of cyanobacteria supports shallow water conditions (Fig. 2C).

Bulk sample XRD analyses of six samples indicate dolomite, calcite, goethite, hematite, quartz, and mica (muscovite) as the main minerals. The distribution of minerals according to profiles was determined based on high-resolution micro-Raman analyses. The main components detected (dolomite, quartz, calcite, goethite, hematite, and carbonaceous material) were used for further investigations. The distribution of carbonaceous material in the samples is inhomogeneous, often occurring as patches. Occasionally, pyrite (μm-size) with organic matter, apatite, rutile, anatase, quartz (matrix material and very rarely debris), and feldspar

(debris-very rare) were also detected. Muscovite occurs in smaller-larger quartz enrichments. Rutile and anatase belong to quartz-rich goethitic parts, whereas apatite occurs in goethite-rich parts of iron stromatolite-like microbial structures.
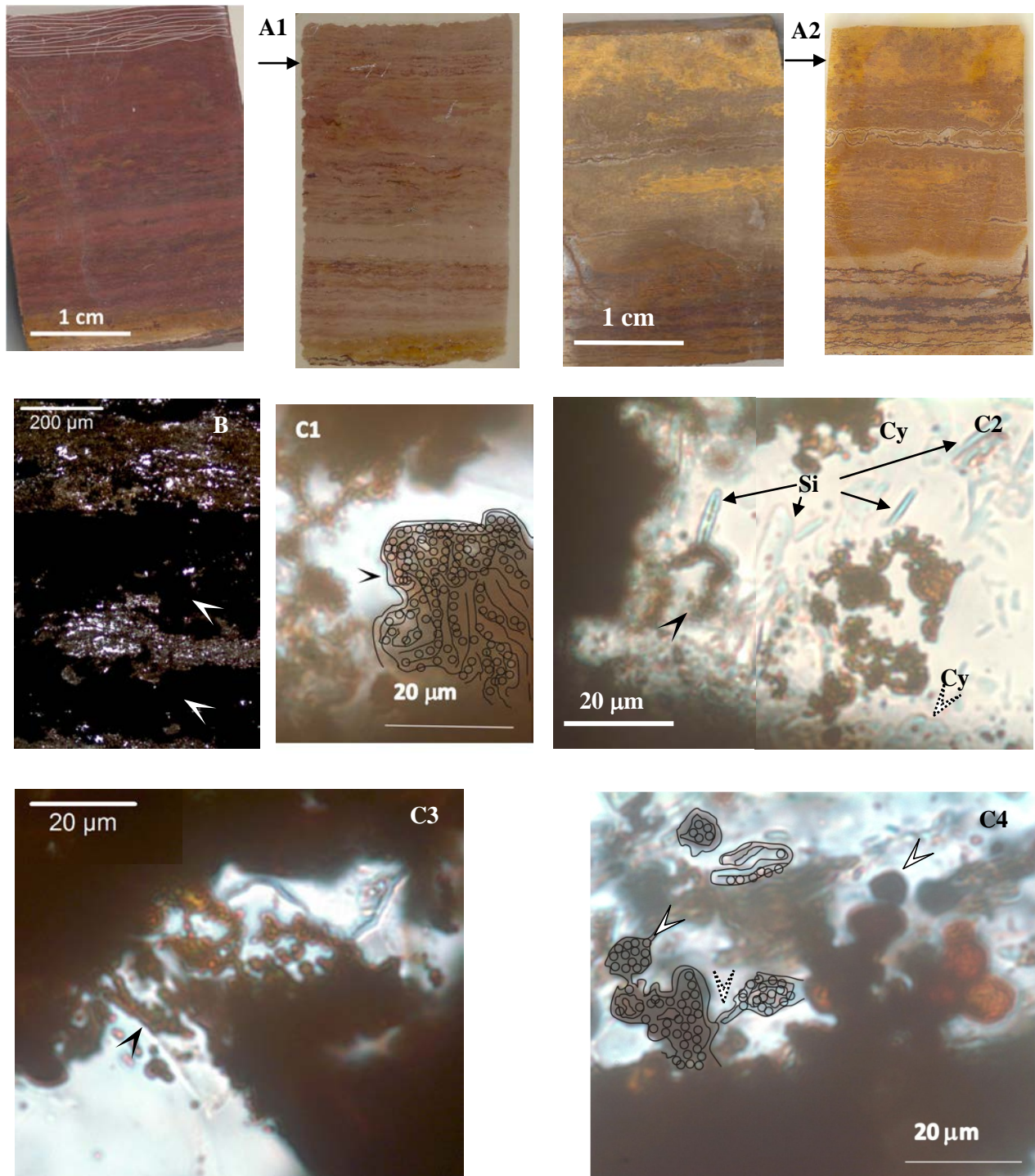

Figure 2. Polished sample and thin section photos showing Fe-rich biomat structures (goethite and hematite) for different representative samples (*C12; C13a1, C13b1, C13b2, C13c*) and magnifications (the density of the biomats is variable). (A1-A2) Photos of polished surfaces of samples and thin sections, arrows show from polished surfaces to thin sections; (A1)-*sample C13c*, (A2)-*C12*; (B) Section of Fe-rich biomat, thin section photo, 1Nicol, sample C12, arrows show opaque mineralized segments; (C1-C4) Fe-rich mineralized filamentous (tubular) microbial forms (black arrows), unnamed colonial coccoid cells, spheroidal unicells, sheath-enclosed colonial unicells (white arrows), (C1)-*sample C12*, (C2)-*C13a1*, (C3)-*C13b2*, (C4)-*C13b1*; Si on C2 indicates silica-bearing fossils; Cy indicate cyanobacteria; the matrix material is quartz, dolomite and hydromuscovite, thin section photos, 1Nicol. Some features in photos A1, C2, and C4 were graphically enhanced for better recognition due to low contrast of the photographs.

Raman spectra allowed the identification and distribution of microbially mediated minerals (goethite and hematite, formerly ferrihydrite) in samples C13b2 and C13c.

Sample C13b2 reveals a strongly mineralized series of Fe-rich laminae (assumed biomats) in a matrix of quartz and C13c represents the basal transition to the local cap dolomite lithology (Fig. 3). Our calculation of the supposed Fe-biomat laminae was made by visual counting.

Thin section C13b2 represents both thinner (100-200 μm) and thicker Fe-rich laminae (up to ~ 1 mm, Fig. 3A). The thinner ones are more common. Some biomat layers contain only goethite or hematite, whereas others contain both minerals. Thicker goethitic biomats occur in the lower part of section 2 and the top of section 3. The abundance of carbonaceous material was not determined in the studied sections, but small patches of organic material are present in the sample. Calcite is rare, mostly occurring in the form of debris material. Visual counting resulted in 100 laminae in the thin section (18.5 mm thick). Using this number, the average thickness of the layers is 185 μm (which we rounded to 200 μm for easier calculations).

The distribution and intensity of the laminae in the C13c thin section is variable (Fig. 3B). The lower part of section 1 shows weak authigenic dolomite formation and very intense Fe-rich biomat series (less than 3 mm thick). The dolomite precipitation then increased, resulting in less intense mat formation. Irregular intensity changes characterize the biomat-dolomite formation in the upper part of the thin section. Their thickness variation is approximately 100-200 μm in all sections studied by Raman spectrometry, resulting in 165 laminae within the 33-mm-thick section. Thus we assume an average thickness of 200 μm for this section, too.

5. DISCUSSION

5.1. Synsedimentary Fe-rich biomat formation

The geological record of Neoproterozoic Snowball Earth glaciations in general consists of glacial diamictites, which can contain and/or can be followed by a postglacial transition layer, at its basis rich in Fe/Fe-Mn oxide-clay, and finally covered by thick cap carbonate (Hoffman et al., 2011, e.g., Doushantuo Fm. (China), Rapitan Group (Canada), Jacdigo Group, Brazil). This widespread cap carbonate formations are well studied and microbial contribution in their genesis is generally accepted (Fraiser & Corsetti, 2003). Contrary, only rare information can be found on microbial mediation of the Fe-rich postglacial transition layer (Pruss et al., 2010). In our sections the Sturtian diamictites are followed by Fe-oxide-rich postglacial transition layers and identifying it for the first time as a fossilized biomat is a basically new observation. This study does not support the previously suggested hypotheses, including: (i) leaching/weathering product of diamictite (Hoffman et al., 1998; Hoffman & Schrag, 2002); (ii) extraterrestrial a) extraterrestrial dust (Bodiselitsch et al., 2005), b) impact ejecta (Koeberl et al., 2007); (iii) chemical sediments a) ferrous vs. euxinic anoxia, b) subglacial, sulphate-rich ferrous waters and c) localization of oxidative titration (Hoffman et al., 2011). Optical microscopic investigations (textural and mineralogical) confirmed that our Sturtian transition layer of Steilrandberge (C12) and Sesfontain-Opuwo (C13) sections are not weathered or condensed ones. A condensed section contains non-depositional surfaces, and on that surfaces some erosional features, or, e.g., in case of microbial activity (which occurs at the sediment/water contact zone) would end in a dense border, because with time, open spaces are filled with minerals. Weathered sections would contain altered minerals; clay minerals also indicate diagenesis and/or alteration, but in the studied sections they do not occur, thus the samples do not show any indication of weathering. In the case of our samples, authigenic mineralization took place together with microbial mineralization (quartz and carbonate) which suggest a special type of accumulation. Microbes living in the solution (aquatic environment) were mineralized and matrix minerals were precipitated in intimate connection with microbes, which preserved in a very fine structure (authigenic mineralization). The complex microtextural features (filamentous forms with inner globular fine texture) also exclude inorganic chemical precipitation (Liesegang banding).

In the vicinity of our sample localities the sedimentary environment was dominated by a continental rift setting giving rise for a considerable topographic relief above and below sea-level locally holding domains, with fresh- to brackish-water. We consider that transportation and deposition of massive diamictite material required powerful media such as glacier ice or melt-water rivers, both providing tight influence concerning the water composition within that regions. The reported iron-rich straticulate sedimentary structures formed temporally representing initial sea ice deglaciation as a consequence of melting glaciers. We assume that a photosynthetic zone existed during the formation of the mentioned postglacial transition layer, which may have been rich in cyanobacterial activity at the sediment/water interface.
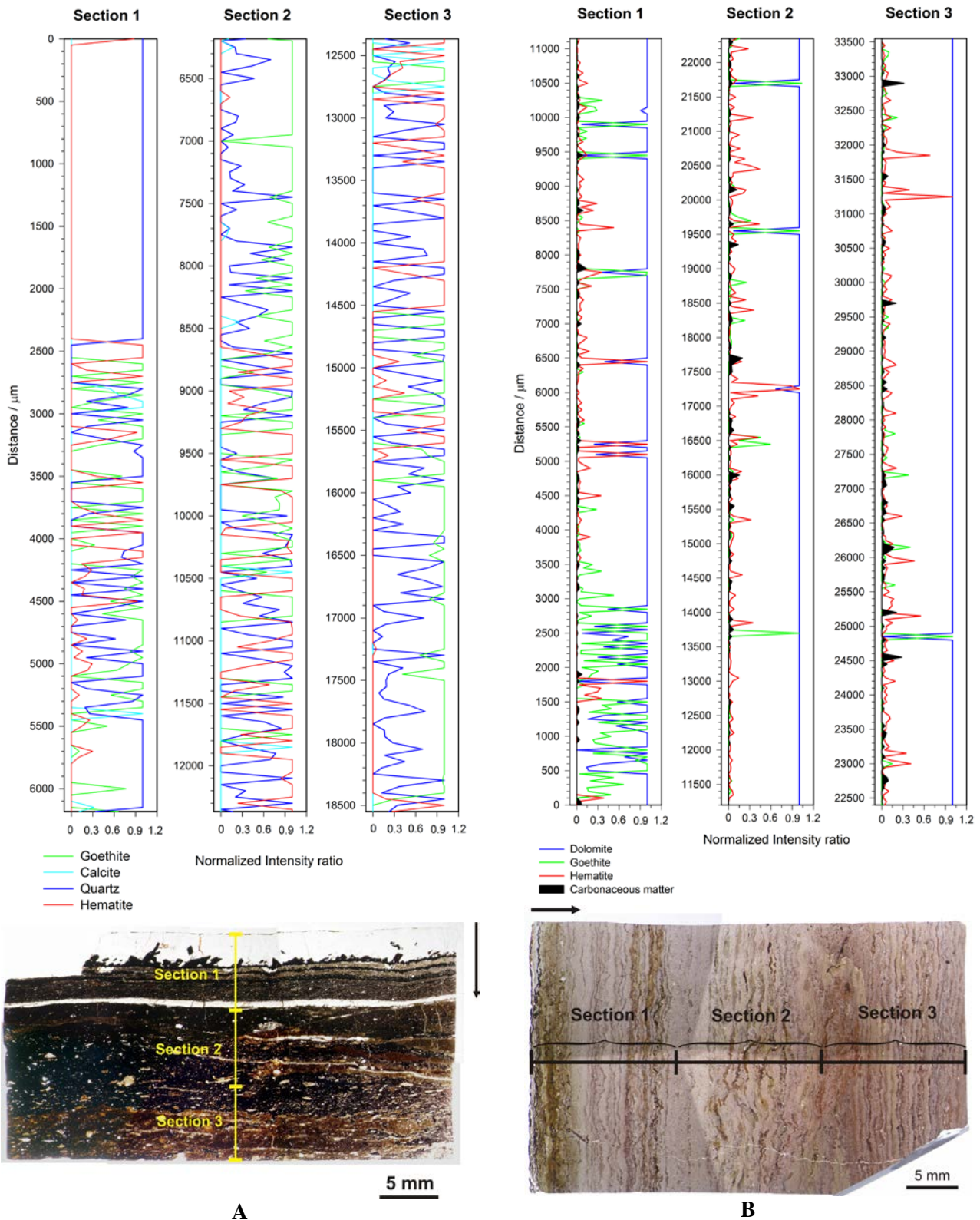
Figure 3. Composite images of C13b2 (A) and C13c (B) oriented thin sections with bands (1-3) of Raman microscopy measurements
The distance between two measured points is 50 µm; Diagrams of relative peak height ratio vs the analytical spot number of each of the 6 phases along the Raman scanned section of the C13b2 and C13c thin sections. Intensity ratios are normalized to the highest peak for each spectrum. The following Raman bands were used for normalization: goethite: ~390 cm^{-1}; hematite ~225 cm^{-1}; quartz: ~463 cm^{-1}; carbonaceous matter: ~1586 cm^{-1}; dolomite: 1097 cm^{-1}; calcite: 1088 cm^{-1}. Number of total Raman spectra: 372 (C13b2) and 660 (C13c).

This environmental assessment is suggested by the observed organic matter distribution in the measured sections of Sturtian transition layers from Sesfontain-Opuwo and Steilrandberge localities and by diverse putative microbial textures, among them features of Fe-free filamentous microbes (Fig. 2C). First of all, we study only the case of the above-mentioned Fe-rich biomat formation for the purpose of their paleoenvironmental interpretation. Then we try to estimate the time necessary for the upgrowth, as it is supposed that MMPSS play an important role in paleoenvironmental considerations.

The basic aim is to confirm the existence of Fe-oxidizing bacteria forming Fe-rich biomats in the samples. The presence of Fe-rich biomats is indicated by textural evidence (Fig. 2C), homogeneous Fe precipitation along the filaments that build a 3D network, which is a robust biosignature (Chan et al., 2011). Understanding the biochemistry of biomat formation is key for determining the type of Fe-rich biomats that may have been involved with the formation of the samples lithology and thus are defining the suspected environmental conditions. There are four types of microbial metabolism that can oxidize Fe^{2+} forming Fe-oxide minerals (Konhauser, 1998). The first type of the microbial Fe(II) metabolisms is acidophilic and oxic, the occurrence of which in shallow fresh- to brackish-water conditions is unlikely. A second type of microbial Fe(II) metabolism is driven by light, anoxic/anaerobic, and neutrophilic (photoferrotroph); a condition that is not supported by the mineralogy. The third type is suboxic/anaerobic, where neutrophilic NO_3 reducers coupled with Fe(II) oxidizers probably contributed to the biochemical milieu, but morphological features do not support this metabolism as main process in biomat formation. The formation conditions were thus most likely governed by the fourth type, namely suboxic and neutrophilic *Gallionella*-like Fe-oxidizing microbes. Non-enzymatic reactions provide an indirect role for bacteria in the oxidation of Fe. As a result of microbial activity, chemical conditions (Eh, pH) are changed in the vicinity of the cells, favoring the chemical oxidation of Fe. Non–Fe-oxidizing microbes may have been the sole microbiota involved in mat formation. The main difficulty with this scenario, however, is the uniformity of the Fe lacework structures throughout the section, which would not be expected to form from inorganic processes.

Thus, two types of Fe-rich biomats are considered as possibilities for what we observe in our samples, all of which are neutrophilic and consistent with shallow fresh- to brackish-water conditions: (1) *Gallionella*-like microbial neutrophilic microaerobic Fe^{2+}-oxidizing bacteria with photosynthetic metabolism (Konhauser, 1998); (2) *Gallionella*-like non-photosynthetic neutrophilic microaerobic microbial Fe^{2+}-oxidizing bacteria (Hallbeck & Pedersen, 1990; Konhauser, 1998). Of the two types of microbial Fe^{2+} oxidation, photosynthetic metabolism produces a daily rhythmicity with growth only during daylight. Biomat growth at the sediment/water interface would have been in competition with authigenic sediment formation. Alternatively, non-photosynthetic microbial Fe^{2+}-oxidizing bacteria can also produce rhythmic developmental stages via existing as free-living Fe^{2+}-oxidizing bacteria in the lag and log phases, and stalk formation (Fe-rich biomat) during the stat phase under optimal conditions. (Microbial population growth phases are the following: (i) *lag phase:* bacterial adaptation; (ii) *log (*logarithmic) *phase:* a period characterized by cell doubling with exponential growth; (iii) *stationary (stat) phase:* the growth rate slows as a result of nutrient depletion and accumulation of toxic products; (iv) *decline (dec) phase:* closes the growth period (exponential death phase), bacteria succumb to their own wastes (but endospores survive), and the cycle starts again (Novick, 1955; Zwietering et al., 1990).

For *Gallionella*-like freshwater and *Mariprofundus*-like marine types, 1–3 weeks (7–21 days) of whole microbial population growth is reported based on laboratory experiments, and natural observations (Hallbeck & Pedersen, 1990; Chan et al., 2011; Polgári et al., 2012).

Microbial mats always form at the sediment/water interface or very close to it (within a few cm), and this fact excludes that these microbial mats formed long after the sediments were deposited; thus they are synsedimentary formations that have important roles in paleoenvironmental interpretation.

The Raman spectra indicate the presence of organic matter in the goethite-hematite lacework (Raman shifts at 1000-2000 cm^{-1}); even though the data are not diagnostic regarding the exact type of organic matter (biomarkers), a biogenic origin of our samples is supported.

The microtextural evidence and the fine-grained authigenic dolomite support a suboxic and neutrophilic environment. Debris did not dilute the sediments, and Fe precipitation in mats via redox interfaces can be excluded based on textural evidence (Gerdes, 2007).

Increasing biomat condensation and 3D mats relate to sediment starvation (lower intensity of authigenic mineralization; Gerdes, 2007). Starving

sedimentary conditions are supported by authigenic carbonate (dolomite) formation, in which debris (quartz, feldspar) is rare. Starving conditions support the formation of well-developed mats generally within 1-3 weeks (Gerdes, 2007), which support our interpretation. Authigenic dolomite formation is supported by a fresh- or brackish-water environment (marine sulfate inhibits the binding of Mg to carbonate) and slightly negative $\delta^{13}C$ values because of the organic matter-rich environment. The dolomite precipitation most likely occurred via microbial mediation (Hoffman et al., 2011). The carbonate is Fe-free, which supports the lack of diagenetic Fe reduction as a main process. Locally very fine-grained pyrite in quartz was observed together with organic matter and most likely formed by decay from the sulphur in organic matter.

Annual, seasonal rhythmicity can be excluded because the weather conditions during biomat formation were in the freezing to just thawing range.

5.2. Diagenesis of Fe-rich biomats

According to the diagenesis of Fe-rich biomats, the microbes produce poorly ordered ferrihydrite as a primary mineral, which transforms to more ordered minerals, such as goethite or hematite, within a few months or years via dissolution-dehydration processes (Konhauser, 1998; Schwertmann & Cornell, 2007). The main Fe oxide mineral in the filaments of our samples is goethite, but Raman analyses indicate that hematite also occurs. The fossilized Fe-rich biomats were rapidly and extensively encrusted by authigenic minerals, such as dolomite and silica, similarly to what has been reported by Baele et al., (2008). The amorphous silica can easily transform into more stable minerals, such as cristobalite, tridymite, and quartz (Herdianita et al., 2000). Silica precipitation is derived by either the destruction of organic complexes or the transformation of ferrihydrite (Baele et al., 2008). Apatite can be precipitated under a pH of 7-8 and occurs in micrometer-sized crystals in the silica-rich part of BIFs. Similar apatite occurrences were noted in our samples, based on Raman analyses. Muscovite (hydromuscovite) is common in the studied samples and was most likely formed by the diagenesis of cyanobacteria filaments in Fe-rich microbialites by the leaching of biofilm alkali (Na, Ka, Al, Mg) (Ewers, 1983).

The organic matter was preserved in the sediment because of the (i) intense authigenic carbonate and Fe oxide mineralization and (ii) the absence of oxidizing agents in the matrix material (absence of Fe reduction because of the stabilization of primary ferrihydrite). The maturation degree of the organic matter is variable in the samples. The sediment formed under suboxic conditions, which later did not turn anoxic. The microbial Fe oxidation ended toward the onset of cap carbonate precipitation, which most likely is due to (i) the elimination of the Fe supply and (ii) the change from suboxic to oxic conditions.

5.3. Constraints on sedimentation rates

So far the timescales for Cryogenian deglaciations have been only specifically abiogene-targeted in climate modeling up to thousand and million years: 10^4-10^5 yr (Hoffman et al., 2007), 10^3 yr (Hyde et al., 2000), 10^4-10^5 yr (Le Hir et al., 2009; Font et al., 2010). In contrast, longer deglaciation times (10^5-10^6 yr) were proposed by, e.g., Trindade et al. (2003), and Raub et al., (2007). The above-mentioned models are based on meteorological simulations, abiogenic precipitation of cap carbonate, geochemical studies, or weathering processes. We propose that cap carbonates as a whole formed after the main deglaciation process and the Fe-rich microbialites emerging at their basis in the studied localities represent the immediate beginning of the deglaciation process. Below the Fe-rich biomat layer is the uppermost part of a diamictite unit, which is thought to be deposited from glacier ice or meltwater rivers in the course of an entire glacial stage during the Cryogenian period, but in any case the onset of these layers marks the cessation of glacially mediated sedimentation processes. The continuously overlying formation is a ~40-m-thick pile of cap-carbonate, which did start with fresh-water to brackish environmental conditions at its very base, but now alter to marine conditions caused by an increasing sea level due to the input of melting inland glacier ice. We suggest that the assumed biogenic-mediated deposition of layers represent distinct chronological periods, thus our results may help with the (local) estimation of postglacial sedimentation rates.

Recent iron-rich biomat formations beneath the sea ice (*Gallionella* with diatoms, and cyanobacteria) at the Earth's polar regions may be a clue that iron favoring biomats possibly have formed during the deglaciation after each glacial stage of the Snowball Earth's period (Vincent & Howard-Williams, 2000). Nevertheless, deglaciation histories suggest that Sturtian and Marinoan ice sheets disappeared rapidly (Hoffman et al., 1998). Based on recent analogs and accumulation rate studies on the Marinoan cap carbonate, the deglaciation took place over a period of several thousand years

(Castanier et al., 2009; Font et al., 2010; Hoffman et al., 2011).

In case of our Sturtian postglacial transition layer samples, microbial layers (series of Fe-rich biomats) were used for the estimation of sedimentation rates at the very beginning of an environmental change due to vanishing sea-glacier ice. Assuming that biomineralization occurs only during some phases of microbial growth, the microbial layering can be used as a time scale (Polgári et al., 2012). Our samples display Fe-rich laminations, suggesting FeOB activity during their deposition. On the other hand, the proposed FeOB occurrence indicates that we need to consider microbial characteristics, such as microbial population growth cycles (in the form of mineralized microbial layering).

The proposed *Gallionella*- or *Mariprofundus*-type Fe-oxidizing bacteria form stalks (filamentous form) (Fe-rich biomats - biomineralization) only during the stat phase of microbial growth cycle and under optimal conditions, producing rhythmic developmental stages via existing, free-living Fe^{2+}-oxidizing bacteria (without mineralization) in the lag and log phases. The mineralized horizons of the Fe-rich biomat represent distances in the sediment that can be measured on micrometer to millimeter scales, explaining how the mineralogical/geochemical composition of these layers can be converted into chronological information. In the layers we consider only the Fe-oxide phase resulting from biomineralization in our calculations. We did not find any evidence for annual lamination, such as rhythmic debris contribution or other mineralogical differentiation. Microbial activity cycles are of much shorter duration (only minutes, days, weeks).

The laminations visible in our samples comprise Fe-rich mineralized parts and less or non-mineralized parts following each other. Naturally, the laminae are not regular in any physical, mathematical, or chemical sense, because many factors influence the microbial metabolism and the 3D filamentous network, but macroscopically they show rhythmicity on a mm-scale. Measuring the length of the mineralized and non-mineralized laminae, the number of laminae can be counted in the studied layer, which is ca. 1.45 m thick in the proximity of the C13 locality, thus providing a basis for our calculations.

The lamina thicknesses in the two measured sections are similar on average (200 µm). Extrapolating the lamina frequency to the whole postglacial transition layer (1.45 m), the estimated number of laminae is 7,250.

The Fe-oxidizing bacterial activity could be driven by light (supported by shallow water conditions) as photosynthetic metabolism; hence the laminae could represent a daily cycle, and, thus represent a minimum estimation for the sediment accumulation of the 1.45-m-thick postglacial transition layer of 7,250 days (18 years). In the Neoproterozoic period the length of years was 400-430 days and the length of days was 22 hours (Williams, 2000), but here we use an average 400 days/year and 22 hours/day.

Otherwise the maximum estimation is a three-week (21 days) duration of the microbial population growth period of non-photosynthetic Fe-oxidizing bacteria, giving a total of 152,250-days (381 years) required for the accumulation of our 1.45 m thick section. Even at the upper range of our estimate, this is a very rapid timescale for deglaciation as represented by the thin Fe-rich postglacial transition layer, and about one tenth of even the shorted estimate mentioned above (10^3 yr, Hyde et al., 2000). The postglacial transition layer does not show evidence for erosion or another hiatus, or other annual or seasonal rhythmicities that could be explained by long-lasting freezing-melting conditions.

At our C13 locality the 1.45-m-thick pile of microbially mediated layers are concordantly overlain by 4 m of thin-bedded planar grain flow deposits. Their successive hanging wall grain flow deposits exhibit sedimentary slumping structures within a ~ 40 – 50 m thick rock sequence. We suggest that this observed sedimentary trend was caused by a gradual, tectonically mediated subsidence of the region. Consequently the environmental conditions of the mentioned microbial layers formation may have been explained by beginning of cap carbonate formation and deglaciation duration. Cap carbonates are generally divided in lower cap dolostone and an upper cap limestone (e.g., James et al., 2001, Hoffman & Schrag, 2002), which implies a non-uniform process of cap carbonate deposition. We propose that the studied putative biolites represent the onset of deglaciation, i.e., the rapid floating sea-ice collapse in the initial deglaciation phase. There are indications that the Cryogenian glaciations had not much disastrous influence on biota (e.g., Gaidos et al., 1999; Olcott et al., 2005; Corsetti et al., 2006; Moczydłowska, 2008). The refugia for life during Snowball Earth glaciations are still debated, but photosynthetic life might have survived in some ice-free areas (e.g., Le Heron, 2012) or on/in ice as photosynthesis in several meter thick permanently ice-covered Antarctic lakes is known (e.g., Hawes & Schwarz 1999). Melting of sea-ice does not induce sea-level rise and would give microbial organisms the opportunity to growth on hard substrate. Former biofilms under thin ice locations and cryoconites

(McMenamin, 2004 and references therein) could now flourish on the continental shelf areas or inland seas. According to Kasemann et al., (2010), the paleoenvironmental conditions during the Sturtian were different from those of the Marinoan; i.e., no extreme pH of the ocean and no elevated pCO_2 at the glaciation and deglaciation time, providing adequate conditions for neutrophilic microbial mats. The duration of continental ice deglaciation, or melting of ground ice, which would have diminished microbial induced sedimentation layers, is not constrained by our study.

6. CONCLUSIONS

We present the first identification of mat-forming filamentous Fe-oxidizing bacteria in the Sturtian postglacial transition layer. The existence of Fe-oxidizing bacterial mats suggests a basically different paleoenvironment (suboxic, neutral) than what was considered for similar widespread Fe-microbialites earlier (anoxic, photoferrotroph, acidophilic microbes). The Sturtian (sea-ice) deglaciation process happened extremely rapidly during deposition of this very thin but important transition layer (few hundred years) based on mineralized bacterial layering.

These results allow comparisons with other Sturtian and Marinoan Fe-bearing layers of variable geological settings and also concerning the paleoenvironmental conditions and the duration of the transition layers formation. It is proposed that the Fe-bearing transitional layer represents the beginning of the deglaciation period. At other localities it can give information on the duration of the formation of Fe-bearing layers.

REFERENCES

Arnaud, E., Halverson, G.P. & Shields-Zhou, G., 2011. Chapter 1 The geological record of Neoproterozoic ice ages. Geological Society, London, Memoirs, 36/1, 1–16.

Baele, J.-M., Bouvain, F., De Jong, J., Matielli, N., Papier, S. & Prat, A., 2008. Iron microbial mats in modern and Phanerozoic environments. Proc. Soc. Phot. Instr. Eng. 7097, 70970N–70970N–12.

Bodiselitsch, B., Koeberl, C., Master, S. & Reimold, W.U., 2005. Estimating duration and intensity of Neoproterozoic Snowball glaciations from Ir anomalies. Science, 308, 239–242.

Campbell, I.H. & Squire, R.J., 2010. The mountains that triggered the Late Neoproterozoic increase in oxygen: The second great oxidation event. Geochim. Cosmochim. Acta, 74, 4187–4206.

Castanier, S., Le Métayer-Levrel, G. & Perthuisot, J.-P., 2009. Ca-carbonates precipitation and limestone genesis — the microbiogeologist point of view. Sedim. Geol., 126, 9–23.

Chan, C.S., Fakra, S.C., Emerson, D., Fleming, E.J. & Edwards, K.J., 2011. Lithotrophic iron-oxidizing bacteria produce organic stalks to control mineral growth: implications for biosignature formation. Multidisciplinary Journal of International Society for Microbial Ecology, 5, 717–727.

Christie-Blick, N., Sohl, L.E. & Kennedy, M.J., 1999. Considering a Neoproterozoic Snowball Earth. Science, 284, 1087–1087.

Corsetti, F. A., Olcott, A. N. & Bakermans, C., 2006. The biotic response to Neoproterozoic snowball Earth. Palaeogeogr., Palaeoclimat., Palaeoecol., 232, 114-130.

Ewers, W.E., 1983. Chemical Factors in the Deposition and Diagenesis of Banded Iron-Formation, in: A.F. Trendall and R.C. Morris (Eds.), Developments in Precambrian Geology, Vol. 6, Iron formation: Facts and Problems. Elsevier, 491–512.

Eyles, N. & Januszczak, N., 2004. "Zipper-rift": a tectonic model for Neoproterozoic glaciations during the breakup of Rodinia after 750 Ma. Earth-Sci. Revs., 65, 1–73.

Fairchild, I.J. & Kennedy, M.J., 2007. Neoproterozoic glaciation in the Earth System. J. Geol. Soc. Lond., 164, 895–921.

Font, E., Nédélec, A., Trindade, R.I.F. & Moreau, C., 2010. Fast or slow melting of the Marinoan snowball Earth? The cap dolostone record. Palaeogeogr., Palaeoclim., Palaeoecol., 295, 215–225.

Fraiser, M.L. & Corsetti, F.A., 2003. Neoproterozoic carbonate shrubs: interplay of microbial activity and unusual environmental conditions in post-Snowball Earth oceans. Palaios, 18, 378–387.

Gaidos, E.J., Nealson, K.H. & Kirschvink J.L., 1999. Life on ice-covered oceans. Science, 284, 1631-1633.

Gerdes, G., 2007. Structures left by modern microbial mats in their host sediments. In: Schieber, J., Bose, P.K., Eriksson, P.G., Banerjee, S., Sarkar, S., Altermann, W., Catuneanu, O. (Eds.) Atlas of Microbial Mat Features Preserved within the Siliciclastic Rock Record. Elsevier, 5-38.

Hallbeck, L. & Pedersen, K., 1990. Culture parameters regulating stalk formation and growth rate of Gallionella ferruginea. J. Gen. Microbiol., 136, 1675–1680.

Harland, W.B. & Rudwick, M.J.S., 1964. The great infra-Cambrian ice age. Scientific American, 211, 28-36.

Hawes, I. & Schwarz, A.M., 1999. Photosynthesis in an extreme shade environment: benthic microbial mats from Lake Hoare, a permanently ice-covered Antarctic lake. J. Phycol., 35/3, 448-459.

Herdianita, N.R., Browne, P.R.L., Rodgers, K.A. & Campbell, K.A., 2000. Mineralogical and textural changes accompanying ageing of silica sinter. Miner. Deposita, 35, 48–62.

Hoffman, P.F., 2002. Carbonates bounding glacial deposits: Evidence for Snowball Earth episodes and greenhouse aftermaths in the Neoproterozoic Otavi Group of northern Namibia. Excursion Guide, 16th International Sedimentological Conference, Auckland Park, South Africa, 39 p.

Hoffman, P.F. & Halverson, G.P., 2008. Otavi Group of the western Northern Platform, the Eastern Kaoko Zone and the western Northern Margin Zone. In: Miller R.M. and Becker, T. (Eds.) The Geology of Namibia: Neoproterozoic to lower Palaeozoic. Vol. 2, Geological Survey of Namibia (Windhoek), 69-136.

Hoffman, P.F. & Li, Z.-X., 2009. A palaeogeographic context for Neoproterozoic glaciation. Palaeogeogr., Palaeoclim., Palaeoecol., 277, 158–172.

Hoffman, P.F. & Schrag, D.P., 2002. The snowball Earth hypothesis: testing the limits of global change. Terra Nova, 14, 129–155.

Hoffman, P.F., Kaufman, A.J., Halverson, G.P. & Schrag, D.P., 1998. A Neoproterozoic Snowball Earth. Science, 281, 1342–1346.

Hoffman, P.F., Halverson, G.P., Domack, E.W., Husson, J.M., Higgins, J.A. & Schrag, D., 2007. Are basal Ediacaran (635 Ma) post-glacial "cap dolostones" diachronous? Earth Planet. Sci. Lett., 258, 114-131.

Hoffman, P.F., Macdonald, F.A. & Halverson, G.P., 2011. Chemical sediments associated with Neoproterozoic glaciation: iron formation, cap carbonate, barite and phosphorite. Geological Society, London, Memoirs, 36, 67–80.

Hyde, W.T., Crowley, T.J., Baum, S.K. & Peltier, W.R., 2000. Neoproterozoic "snowball Earth" simulations with a coupled climate/ice-sheet model. Nature, 405, 425–429.

James, N.P., Narbonne, G.M. & Kyser, T. K., 2001. Late Neoproterozoic cap carbonates: Mackenzie Mountains, northwestern Canada: precipitation and global glacial meltdown. Can. J. Earth Sci., 38, 1229-1262.

Joint Committee on Powder Diffraction Standards database (JCPDS), 1980.

Kappler, A., Pasquero, C., Konhauser, K.O. & Newman, D.K., 2005. Deposition of banded iron formations by anoxygenic phototrophic Fe(II)-oxidizing bacteria. Geology, 33, 865–868.

Kasemann, S.A., Prave, A.R., Fallick, A.E., Hawkesworth, C.J. & Hofmann, K.H., 2010. Neoproterozoic ice ages, boron isotopes, and ocean acidification: Implications for a snowball Earth Geology, 38, 775-778.

Kennedy, M.J., Runnegar, B., Prave, A.R., Hoffmann, K.-H. & Arthur, M.A., 1998. Two or four Neoproterozoic glaciations? Geology, 26, 1059–1063.

Kirschvink, J.L., 1992. Late Proterozoic low-latitude glaciations. In: Schopf, J.W. (Ed.) The Proterozoic Biosphere. Cambridge University Press, Cambridge, 51-52.

Klein, C. & Beukes, N.J., 1993. Sedimentology and geochemistry of the glaciogenic late Proterozoic Rapitan Iron-Formation in Canada. Econ. Geol., 88, 542–565.

Klein, C. & Ladeira, E.A., 2004. Geochemistry and mineralogy of Neoproterozoic banded iron-Formations and some selected, siliceous manganese formations from the Urucum District, Mato Grosso Do Sul, Brazil. Econ. Geol., 99, 1233–1244.

Koeberl, C., Ivanov, B.A. & Goodman, J., 2007. Impact-induced deglaciation of the Snowball Earth? AGU Fall Meeting Abs., #U22A-08. Bibliographic Code: 2007AGUFM.U22A.08K.

Konhauser, K.O., 1998. Diversity of bacterial iron mineralization. Earth-Sci. Rev., 43, 91–121.

Konhauser, K.O., Hamade, T., Raiswell, R., Morris, R.C., Ferris, F.G., Southam, G. & Canfield, D.E., 2002. Could bacteria have formed the Precambrian banded iron formations? Geology, 30, 1079–1082.

Knoll, A.H., 2003. The geological consequences of evolution. Geobiology, 1/1, 3–14.

Le Heron, D.P., 2012. The location and styles of ice-free 'oases' during Neoproterozoic glaciations with evolutionary implications. Geosciences, 2, 90–108.

Le Hir, G., Donnadieu, Y., Goddéris, Y., Pierrehumbert, R.T., Halverson, G.P., Macouin, M., Nédélec, A. & Ramstein, G., 2009. The snowball Earth aftermath: Exploring the limits of continental weathering processes. Earth Planet. Sci. Lett., 277, 453–463.

Martin, H., 1964. Beobachtungen zum Problem der jung-Präkambrischen glazialen Ablagerungen in Südwestafrika. Geologische Rundschau, 54, 115–127.

McMenamin, M.A.S., 2004. Climate, paleoecology and abrupt change during the Late Proterozoic: A consideration of causes and effects. In: Jenkins, G.S., McMenamin, M.A.S., McKay, C.P., Sohl, L. (Eds.) The Extreme Proterozoic: Geology, Geochemistry, and Climate. American Geophysical Union, Washington, D C., Geophys. Monogr. Series 146, 215-229.

Moczydłowska, M., 2008. The Ediacaran microbiota and the survival of Snowball Earth conditions. Precambr. Res., 167, 1-15.

Noffke, N., Knoll, A.H. & Grotzinger, J.P., 2002. Sedimentary controls on the formation and preservation of microbial mats in siliciclastic deposits: A case study from the upper Neoproterozoic Nama Group, Namibia. Palaios, 17, 533–544.

Noffke, N., Gerdes, G. & Klenke, T., 2003. Benthic cyanobacteria and their influence on the sedimentary dynamics of peritidal depositional systems (siliciclastic, evaporitic salty, and evaporitic carbonatic). Earth-Sci. Rev., 62, 163–176.

Noffke, N., Eriksson, K.A., Hazen, R.M. & Simpson, E.L., 2006. A new window into Early Archean life: Microbial mats in Earth's oldest siliciclastic tidal deposits (3.2 Ga Moodies Group, South Africa). Geology, 34, 253–256.

Novick, A., 1955. Growth of Bacteria. Ann. Rev. Microbiol. 9, 97-110.

Olcott, A.N., Sessions, A.L., Corsetti, F.A., Kaufman, A.J & Oliviera, T.F., 2005. Biomarker evidence for photosynthesis during Neoproterozoic glaciation. Science, 310, 471-474.

Polgári, M., Hein, J.R., Tóth, A.L., Pál-Molnár, E., Vigh, T., Bíró, L. & Fintor, K., 2012. Microbial action formed Jurassic Mn-carbonate ore deposit in only a few hundred years (Úrkút, Hungary). Geology, 40, 903–906.

Pruss, S.B., Bosak, T., Macdonald, F.A., McLane, M. & Hoffman, P.F., 2010. Microbial facies in a Sturtian cap carbonate, the Rasthof Formation, Otavi Group, northern Namibia. Precambr. Res., 181, 187–198.

Raub, T.D., Evans, D.A.D. & Smirnov, A.V., 2007. Siliciclastic prelude to Elatina–Nuccaleena deglaciation: lithostratigraphy and rock magnetism through the base of the Ediacaran system. In: Vickers-Rich, P., Komarower, P. (eds) The Rise and Fall of the Ediacaran Biota. Geological Society, London, Special Publications, 286, 53–76.

Schopf, J.W., 2004. Earth´s earliest biosphere: status of the hunt. In: Eriksson, P.G., Altermann, W., Nelson, D.R., Mueller, W., Catuneanu, O. (Eds.) The Precambrian Earth: Tempos and Events. Developments in Precambrian Geology, Elsevier, 516–538.

Schwertmann, U. & Cornell, R.M., 2007. Iron Oxides in the Laboratory: Preparation and Characterization. Wiley-VCH, 188 p.

Trindade, R.I.F., Font, E., D'Agrella-Filho, M.S., Nogueira, A.C.R. & Riccomini, C., 2003. Low-latitude and multiple geomagnetic reversals in the Neoproterozoic Puga cap carbonate, Amazon craton. Terra Nova, 15, 441–446.

Vincent, W.F. & Howard-Williams, C., 2000. Life on Snowball Earth. Science, 287, 2421–2421.

Vincent, W.F., Gibson, J.A.E., Pienitz, R., Villeneuve, V., Broady, P.A., Hamilton, P.B. & Howard-Williams, C., 2000. Ice shelf microbial ecosystems in the high Arctic and implications for life on Snowball Earth. Naturwissenschaften, 87, 137–141.

Whitten, G.F., 1970. The investigation and exploration of the Razorback Ridge iron deposits. Geol. Surv. South Austr., Rep. Invest., 33, 151 p.

Williams, G.E., 1975. Late Precambrian glacial climate and the Earth's obliquity. Geol. Mag., 112, 441–465.

Williams, G.E., 2000. Geological constraints on the Precambrian history of Earth's rotation and the Moon's orbit. Rev. Geophys., 38, 37–59.

Zwietering, M.H., Jongenburger I, Rombouts F.M. & van Riet T.K., 1990. Modeling of the bacterial growth curve". Appl. Envir. Microbiol., 56, 1875–1881.